Tellus (1995), 47B, 145–169
Printed in Belgium – all rights reserved

TELLUS
ISSN 0280–6509

Seasonal uptake of anthropogenic CO_2 in an ocean general circulation model

By NICHOLAS K. TAYLOR, *Hadley Centre for Climate Prediction and Research, Meteorological Office, London Road, Bracknell, UK*

(Manuscript received 1 November 1993; in final form 22 August 1994)

ABSTRACT

A model of the inorganic carbon cycle, embedded within an ocean general circulation model is described, and results from a seasonal simulation of the present-day ocean carbon cycle are presented. Whilst the circulation characteristics of the model appear reasonable, the model gives North Atlantic Deep Water rates that are too low compared with deep water of southern origin, which may result in an overestimate of the southern hemisphere uptake. A comparison of the model results with available observations of dissolved inorganic carbon and partial pressure of carbon dioxide reveals that a defect in the present model is the neglect of ocean biology, which causes the phase of seasonal variations in partial pressure in high latitudes to be incorrectly simulated. A series of experiments were performed in which CO_2 was added to the atmosphere at a specific rate to simulate anthropogenic emissions. The model predicts an oceanic uptake of 44% of atmospheric emissions at the end of a 50-year run. The largest sinks in the model occur in the southern hemisphere and equatorial regions. A comparison between parallel runs made under conditions of seasonally varying and annual-mean forcing reveals that the use of seasonal forcing in the present model makes little difference to the estimate of global oceanic uptake of anthropogenic CO_2. Varying the background coefficient of vertical diffusion, within commonly accepted limits, is found to have a much greater impact on CO_2 uptake estimates.

1. Introduction

The past, present and future movements of carbon between its various source and sinks needs to be known in some detail if we are to be able to predict the course of future climate change. When attempting to make predictions of future climate using coupled ocean-atmosphere general circulation models (GCMs) it is desirable to have a model which is able to take account of feedbacks and which can compute the concentration of CO_2 in the atmosphere as a response to climate change. Another reason for having such a model is that remarkably little is understood about the workings of today's global carbon cycle system. There is a need for more and better estimates of the sink strength of the ocean for anthropogenic CO_2. More accurate esimates of the role of the ocean as a sink for atmospheric CO_2 will also serve to constrain the net effect of the terrestrial biosphere which is even more difficult to quantify than the ocean.

This paper describes integrations made with a global carbon cycle model coupled to a 3-dimensional ocean GCM. The model used can be run coupled to an atmospheric GCM for investigation of feedbacks from the carbon cycle to the climate system, although in the present study we use prescribed climatological atmospheric forcing. The model described here includes only the physical and chemical mechanisms of carbon uptake operating on timescales up to a thousand years. No attempt is made to model the effect of ocean biology on the uptake of atmospheric carbon, nor do we consider the terrestrial carbon cycle, or processes thought to be important on geological timescales. The neglect of biology can be justified on the grounds that we are mainly interested in the uptake of anthropogenic CO_2, which involves looking at the difference between simulations with

Tellus B/47/1/2-10

and without additional CO_2 added to the atmosphere. The effect of biology is assumed to be the same in both cases. This is a reasonable assumption if biological productivity is limited by lack of nutrients over much of the ocean so that the biological pump will be essentially unaffected by increased atmospheric CO_2 levels. This assumption is not necessarily correct, however, as it neglects the role of feedbacks between the biological pump and the climate system, but is nevertheless a useful starting point. The effect of terrestrial biota as a net source or sink of CO_2 is a moot point. Keeling and Shertz (1992) have sought to place constraints on its role by measuring oxygen to nitrogen ratios, and conclude that the effect of deforestation is roughly compensated by the carbon fertilisation effect, although the errors involved in this calculation are as yet very large. Future versions of the model will simulate nutrient, phytoplankton and zooplankton concentrations and their effect on the flux of carbon between surface and intermediate and deep waters. A model of the land carbon cycle is also under development. The present model will serve as a useful yardstick against which later models can be compared.

A more serious omission is the neglect of important feedback mechanisms in the model. The experiment described below in which anthropogenic CO_2 is added to the atmosphere assumes that the ocean is forced in exactly the same way with extra CO_2 as it was before the CO_2 was added. In other words, we ignore the effect that any climate change might have on the operation of the carbon cycle. There are a number of potential feedbacks between the carbon cycle and climate change/global warming, involving, amongst other things, increased sea surface temperature and hence increased pCO_2, changes in the rate of deep water formation, changes in surface fluxes due to changed wind patterns as well as the biological feedbacks just mentioned. Taylor (1992) gives a more complete list of possible feedbacks. The proper investigation of these mechanisms would require the carbon cycle model to be incorporated into a coupled atmosphere-ocean model, the development of which is one of the ultimate aims of this work.

3-D simulations of the ocean carbon cycle have previously been reported using the Geophysical Fluid Dynamics Laboratory (GFDL) ocean model (Sarmiento et al., 1992) and the Hamburg large-scale geostrophic GCM (Maier-Reimer and Hasselmann, 1987; Bacastow and Maier-Reimer, 1990). In these models atmospheric CO_2 forcing is provided by either a time-series of the historical fossil fuel production or by an imposed atmospheric CO_2 concentration history. In this study we take a somewhat different approach. Instead of simulating a particular historical period, we ask the following question: what proportion of a given amount of fossil fuel emitted to the atmosphere is the ocean capable of absorbing over a timescale of 50 years? To answer this, we spin up a coupled ocean-carbon cycle model until it is in equilibrium with an imposed atmospheric concentration of 348 ppm. We then proceed to add CO_2 to the atmosphere at a constant rate and observe the uptake of this additional CO_2 by the ocean. Both seasonal and annual-mean simulations are performed and the results compared. Finally, we look at the effect of changing the vertical diffusion characteristics of the model on uptake of CO_2. The approach adopted, whilst appropriate for studying the response of the model to an atmospheric CO_2 perturbation, is somewhat non-standard and this makes comparison with other models difficult. We are also carrying out a series of simulations under more conventional forcing conditions for the purpose of model intercomparison, and these will be published separately.

The model is described in Section 2. Section 3 describes the model spin-up. The behaviour of the circulation model is discussed in Section 4.1. Subsection 4.2 describes the carbon cycle results under seasonal forcing conditions, and presents results from a seasonal integration in which the uptake of anthropogenic CO_2 by the ocean is calculated. These results are compared with results from a similar run using annual mean forcing in Subsection 4.3, and in Subsection 4.4 we look at the sensitivity of the modelled uptake to the coefficient of vertical diffusion, a poorly-known parameter. Results are summarised in Section 5.

2. Model description

2.1. Ocean circulation model

The ocean circulation model used is based upon the 3-D primitive equation model described by Bryan (1969) and Cox (1984). A detailed descrip-

tion of the equations and their method of solution can be found in the above references. The model is global and includes a realistic approximation to bottom topography and continental coastlines. A horizontal grid resolution of 2.5° latitude by 3.75° longitude was chosen to match the resolution of the Hadley Centre atmospheric climate model (Murphy, 1994). 20 levels are used in the vertical with 7 levels covering the top 113 metres (Table 1). A Kraus–Turner type bulk mixed layer model (Kraus and Turner, 1967) is incorporated within the ocean model in order to improve the simulation of the seasonal cycle of sea surface temperature and mixed layer depths (Ineson and Gordon, 1989). In the present version of the model, SST is not permitted to drift far away from observations (see below), but future versions will be coupled to an atmospheric GCM, and it will then become important to reduce errors in simulating seasonal changes in SST. Below the mixed layer the simple convective mixing scheme described by Cox (1984) is used.

As well as the Kraus–Turner scheme, we use the K-theory mixing scheme of Pacanowski and Philander (1981) to parameterize Richardson-Number-dependent vertical turbulent mixing.

Table 1. *Model levels*

Level	Thickness (m)	Depth of level bottom (m)	Depth of mid-point (m)
1	10.0	10.0	5.0
2	10.0	20.0	15.0
3	10.0	30.0	25.0
4	10.2	40.2	35.1
5	15.3	55.5	47.8
6	23.0	78.5	67.0
7	34.5	113.0	95.7
8	51.8	164.8	138.9
9	77.8	242.6	203.7
10	116.8	359.4	301.0
11	175.3	534.7	447.0
12	263.2	797.9	666.3
13	395.3	1193.2	995.5
14	615.3	1808.5	1500.8
15	615.3	2423.8	2116.1
16	615.3	3039.1	2731.3
17	615.3	3654.4	3346.6
18	615.3	4269.7	3961.9
19	615.3	4885.0	4577.1
20	615.3	5500.3	5192.4

When used in conjunction with the Kraus–Turner scheme, K-theory mixing has little influence on the vertical profiles of temperature and salinity, but it serves the purpose of mixing momentum downwards. This is a necessary feature of a model that has such a high near-surface resolution. When it is left out, wind-driven Ekman currents are confined to the top-most layer and are in consequence too strong (C. Gordon, personal communication). Minimum background values of the eddy viscosity and diffusivity are chosen as $0.1\ cm^2\ s^{-1}$ and $0.5\ cm^2\ s^{-1}$, respectively. Below the thermocline the values used by the model are essentially the background ones. The background vertical mixing coefficient for tracers lies towards the middle of the range of values typically used (0.1 to $1.3\ cm^2\ s^{-1}$), and was chosen in order to avoid numerical problems which can occur when a non-uniform vertical grid is used. Yin and Fung (1991) have shown that a negative effective vertical diffusivity may be produced in regions of strong downwelling when a low value of diffusivity is combined with variable grid spacing, such as that used here. One way around the problem is to increase the explicit vertical diffusivity, which is the approach taken in this study. We also performed one integration using a smaller value of the diffusion coefficient, $0.1\ cm^2\ s^{-1}$, in order to assess the sensitivity of the results to vertical diffusion.

A parameterization of isopycnal diffusion (Redi, 1982; Cox, 1987) is included so that the dominant direction of mixing for tracers such as heat, salt and carbon lies along surfaces of constant density rather than the horizontal. England (1993) found that the inclusion of an isopycnal mixing scheme resulted in an improvement in the simulated production of intermediate water. As in Bryan and Lewis (1979), the isopycnal diffusivity for tracers is assumed to be greater in the upper ocean than in the deep ocean. In addition to the isopycnal component of diffusivity, a small background horizontal coefficient is included to maintain numerical stability.

Because of the convergence of meridians at high latitudes, horizontal viscosity is decreased away from the equator according to:

$$A_m = A_{m1} + A_{m2} \cos \phi \qquad (1)$$

where ϕ is latitude. The smaller coefficient of viscosity at the poles enables a longer timestep to

be used without violating the grid cell Reynolds number stability criterion.

The selection of appropriate values for the subgrid scale mixing parameters can be troublesome since these are not well known. The vertical diffusivity of heat, salt and tracers in particular is problematical because the Bryan–Cox model's thermohaline circulation has been shown to be particularly sensitive to the value chosen (Bryan, 1987). Furthermore, Gargett and Holloway (1992) have shown that the model is also sensitive to the relative magnitudes of the diffusion coefficients for heat and salt when separate coefficients are used. A list of parameters used within the model is given in Table 2.

The coarse horizontal resolution means that the Straits of Gibraltar are not resolved by the model grid. However, the Mediterranean Sea is included in the model, and exchange through the straits of Gibraltar is parameterized in a very simple way, using the method described by Manabe and Stouffer (1988). At each timestep the tracer properties of the Atlantic and Mediterranean grid points immediately adjacent to the Straits are fully mixed down to a depth of 1200 metres. In this way a source of Mediterranean water is introduced into the Atlantic at the correct depth.

A further addition to the basic Cox (1984) model is the inclusion of a sea-ice model based on the zero-layer thermodynamic model of Semtner (1976) with a parameterization of leads and polynyas following Hibler (1979). The inclusion of the brine rejection process should give improved deep water formation rates in seasonal simulations. Roberts and Cattle (1989) discuss the performance of the sea-ice model.

The model is forced with Esbensen and Kushnir (1981) heat fluxes and the climatological wind stresses of Hellerman and Rosenstein (1983). Surface fresh water fluxes were obtained by combining the Jaeger (1976) precipitation dataset with evaporation derived from the Esbensen and Kushnir fluxes. In addition to the prescribed heat and salt fluxes, surface values of temperature and salinity are relaxed back towards climatological values using a method equivalent to that of Haney (1971), so that the surface boundary condition takes the form

$$Q(T) = Q(T_c) + \lambda(T - T_c), \tag{2}$$

$$F(S) = F(S_c) + \lambda(S - S_c)/C_p, \tag{3}$$

where $Q(T_c)$, $F(S_c)$ are the climatological heat and salt fluxes for the climatological sea surface temperature (T_c) and sea surface salinity (S_c), and T, S are the surface values of temperature and salinity predicted by the model. T_c are derived from a joint UKMO/Massachussets Institute of Technology dataset of SST (Bottomley et al., 1990), and S_c are taken from Levitus (1982). C_p is the specific heat capacity of seawater in $J\,Kg^{-1}\,K^{-1}$. λ takes the value 40.9 $W\,m^{-2}\,K^{-1}$, which corresponds to a relaxation timescale of about 60 days for a surface mixed layer of depth 50 m. This formulation prevents the surface temperatures and salinities from drifting far away from climatology. Sea-ice depths and concentrations are similarly forced back towards a model-derived climatology to prevent excessive drift.

2.2. *Carbon cycle model*

The present version of the carbon cycle model is designed to be as simple as possible. The 3-dimen-

Table 2. *Ocean model parameter settings*

background vertical eddy viscosity	υ_b	($cm^2\,s^{-1}$)	0.1
background vertical eddy diffusivity	χ_b	($cm^2\,s^{-1}$)	0.1, 0.5
vertical eddy viscosity under conditions of neutral stability	υ_0	($cm^2\,s^{-1}$)	55.0
maximum vertical eddy viscosity under unstable conditions		($cm^2\,s^{-1}$)	100.0
minimum horizontal viscosity	A_{m1}	($cm^2\,s^{-1}$)	1.5×10^9
additional horizontal viscosity at equator	A_{m2}	($cm^2\,s^{-1}$)	1.5×10^9
surface isopycnal diffusivity	A_s	($cm^2\,s^{-1}$)	2.0×10^7
background isopycnal diffusivity	A_b	($cm^2\,s^{-1}$)	0.4×10^7
depth-scale for decay of isopycnal diffusivity to background level		(m)	500.0
maximum slope of isopycnal surfaces			1.0×10^{-2}
background horizontal diffusivity		($cm^2\,s^{-1}$)	8.0×10^5
relaxation coefficient for surface temperature and salinity	λ	($W\,m^{-2}\,K^{-1}$)	40.9

sional distribution of dissolved inorganic carbon is calculated within the interior of the ocean model using

$$\partial C/\partial t + \boldsymbol{u}\cdot\nabla C + w\,\partial C/\partial z = A_h\nabla^2 C + \partial(K_h\,\partial C/\partial z)/\partial z, \quad (4)$$

where C is the concentration of dissolved inorganic carbon, also known as T_{CO_2}. Except for at the surface, T_{CO_2} is thus treated as an additional conservative tracer by the ocean circulation model. The same mixing coefficients are used for T_{CO_2} as for temperature and salinity. Eq. (4) is solved by an on-line, prognostic method. That is, T_{CO_2} is updated at the same time as new velocity, temperature and salinity fields are calculated. An off-line approach to the solution of eq. (4) would be computationally cheaper, but would not be suitable for coupling to an atmospheric model, and would introduce errors owing to the intermittency of convection. Sarmiento et al. (1992) found that an off-line version of their model took up about 10% more carbon than the on-line version.

T_{CO_2} is comprised of 3 components, whose relative abundance is described by the following chemical equilibrium relations:

$$[H_2CO_3] = k_0\,pCO_2^{(oc)}, \quad (5)$$

$$[H^+][HCO_3^-] = k_1[H_2CO_3], \quad (6)$$

$$[H^+][CO_3^{2-}] = k_2[HCO_3^-], \quad (7)$$

where [ ] denotes concentration. H_2CO_3 is carbonic acid and dissolved gaseous CO_2, CO_3^{2-} is the carbonate ion and HCO_3^- is the bicarbonate ion. $pCO_2^{(oc)}$ is the partial pressure exerted by gaseous CO_2 in parts per million by volume (ppm). k_0, k_1 and k_2 are apparent equilibrium constants, which depend on temperature and salinity. The equations given by Peng et al. (1987) are used to calculate the equilibrium constants, and the computational procedure of Bacastow (1981) is then used to compute $pCO_2^{(oc)}$ using k_0, k_1, k_2, T_{CO_2} and alkalinity. The Peng et al. (1987) equations use dissociation constants determined by Mehrbach et al. (1973). These have been superceded by the more recent measurements of Goyet and Poisson (1989), which are thought to be more accurate. For the purposes of this paper, the differences are very small. Apart from carbonate and bicarbonate ions, borate contributes about 5% to alkalinity and so a correction for borate ion concentration is applied. The variable degree of dissociation of the borate system is also accounted for. Alkalinity is not treated as an additional tracer in this model, since the exclusion of biology means that the processes which can modify it, such as photosynthesis and the removal of calcium carbonate to form shells, are not included in the simulations described here. Exchange of CO_2 with the atmosphere does not alter the sea surface alkalinity because CO_2 is uncharged. A constant value of alkalinity of 2300 μeq kg^{-1} is used, corresponding to an average salinity of 35 psu.

The flux of carbon dioxide between atmosphere and ocean is expressed as the product of a gas transfer coefficient and the partial pressure difference between air and water (Etcheto and Merlivat, 1988; Tans et al., 1990; Thomas et al., 1988):

$$\text{flux} = V_p k_0(pCO_2^{(atm)} - pCO_2^{(oc)}) = V_p k_0\,\Delta pCO_2, \quad (8)$$

where k_0 is the CO_2 solubility given above, $pCO_2^{(atm)}$ and $pCO_2^{(oc)}$ are the partial presures in the atmosphere and the ocean, and V_p is a piston velocity. The product $V_p k_0$ is the gas transfer coefficient. In the experiments reported here the atmospheric pCO_2 is either held constant, or else the atmosphere is treated as a single well-mixed box. Spatial variations in atmospheric pCO_2 are thus neglected, which is a reasonable approximation for simulations which neglect seasonal variation since the lower atmosphere becomes well-mixed over a timescale of about a year (IPCC, 1990). The observed annual mean concentration difference between northern and southern hemispheres is 4 to 5 ppm. The southern hemisphere shows little annual variation in atmospheric CO_2 whilst the northern hemisphere shows variations of up to 10 ppm peak-to-peak amplitude towards the poles, which is thought to be due to seasonal changes in plant metabolism (Pearman et al., 1983). For seasonal simulations the neglect of atmospheric variations may therefore lead to errors in the calculated ΔpCO_2 of several ppm in some places but this is small when compared with the observed values of up to 100 ppm. Seasonal changes in air-sea exchange are dominated by variations in the oceanic partial pressure. A more complete treatment of air-sea

exchange would require the use of an atmospheric transport model and the inclusion of the terrestrial biosphere, which is beyond the scope of this paper.

The piston velocity, V_p, is computed from wind-speed according to the Liss and Merlivat (1986) formulation:

$$\begin{aligned} V_p &= (S_c/600)^{-2/3}\, 0.17U \\ &\quad U < 3.6\ \mathrm{ms}^{-1}, \\ V_p &= (S_c/600)^{-1/2}\, (2.85U - 9.65) \\ &\quad 3.6\ \mathrm{ms}^{-1} \leqslant U < 13.0\ \mathrm{ms}^{-1}, \\ V_p &= (S_c/600)^{-1/2}\, (5.9U - 49.3) \\ &\quad 13.0\ \mathrm{ms}^{-1} \leqslant U, \end{aligned} \tag{9}$$

where S_c is the Schmidt number. The Schmidt number is a measure of the competing effects of gas diffusion and fluid viscosity on gas transfer and is calculated from the formula given by Wanninkhof (1992):

$$S_c = 2073.1 - 125.62T + 3.6276T^2 - 0.043219T^3. \tag{10}$$

Apart from its direct effects on pCO_2 (higher temperatures cause high values of pCO_2), temperature affects the flux across the air-sea interface. High temperatures result in low solubility and a lowering of the flux into the ocean, which is partially offset by an increased flux due to a decreased Schmidt number. The piston velocity increases with increasing wind-speed, an abrupt increase in flux as wind speed exceeds 13 ms^{-1} represents the increase in turbulence brought about by breaking waves. Owing to the non-linearity of eq. (9), for any given averaging period, a piston velocity calculated using an average wind speed will tend to be less than the average piston velocity for that period. Thus the use of monthly climatological winds to force the model will result in an underestimate of the gas transfer as compared with the case where the winds are variable. Wanninkhof (1992) has recently produced a new formulation of piston velocity which gives somewhat higher values than the ones used here. However, sensitivity studies by Sarmiento et al. (1992) showed that, for annual mean forcing at least, global CO_2 uptake is relatively insensitive to the gas exchange formulation. We therefore retain the Liss and Merlivat (1986) formulation, which is commonly used. Over regions of the ocean covered by sea-ice, the atmosphere-ocean flux is drastically reduced since the flux at each grid box given by eq. (8) is multiplied by the ice-free fractional area of that grid box. The only communication between ocean and atmosphere at ice points is through the small portion of a grid box representing leads and polynyas.

In addition to T_{CO_2}, ^{14}C is included as a passive tracer in a similar manner to that used by Toggweiler et al. (1989), using a half-life of 5730 years and an arbitrary fixed atmospheric composition of 100 model units to represent the pre-industrial atmosphere. Results are reported in the conventional units as the per mil difference from the $^{14}C/C$ ratio of the pre-industrial atmosphere by the conversion

$$\Delta^{14}C = (\text{model units} - 100)/10. \tag{11}$$

The gas exchange rate is variable, according to the wind-speed dependent piston velocity computed in eq. (9).

3. Experiments

Initial fields of temperature and salinity were set from the Levitus (1982) climatology, T_{CO_2} was initialised to a constant value of 2300 μmol kg^{-1}, $\Delta^{14}C$ was set to $-150^{o}/_{oo}$, and the model was spun up from a state of rest using the spin-up acceleration techniques described by Bryan (1984). In these, the model physics are distorted by taking a longer timestep for tracers than for the momentum equation and by taking longer timesteps at depth. This can be done because stability criteria are less severe for tracers and at depth within the ocean. The effect of the longer timestep at depth is to increase the effective integration time of the deep ocean relative to the surface. These techniques introduce scaling factors into the time-dependent terms of the equations of motion, which tend towards zero as equilibrium is reached ($\mathrm{d}/\mathrm{d}t = 0$). Thus the equilibium state of a model integrated using spin-up acceleration will be the same as that of a model integrated with standard time-stepping, provided that the forcing used is steady. This results in a considerable saving in computer resources.

The model was spun up with accelerated timestepping for 1200 surface years (equivalent to 9600 years in the deep ocean) using annual-mean forcing (spin-up stage I). Then synchronous timestepping was adopted with the same timestep being used at all depths and the spin-up was continued for a further 50 years (spin-up stage II). Atmospheric pCO_2 was held at a constant value of 348 ppm for the duration of the spin-up, corresponding to the value observed during the middle period of the 1980's. From year 1250 the model was integrated for a further 36 years with seasonal forcing imposed (spin-up stage III). By the end of the spin-up run the model property distributions had reached essentially steady state and the upper layers had come into equilibrium with the imposed seasonal forcing and atmospheric partial pressure (see discussion in Subsection 4.1). By this time the net ocean-atmosphere carbon exchange was less than 0.05 GtC yr^{-1}.

Starting from the end of the seasonal spin-up (stage III) at model year 1286 an experiment was performed in which the atmospheric pCO_2 was no longer prescribed, but was allowed to vary as it exchanged CO_2 with the ocean. This will be referred to as experiment A. For the purposes of this run, the atmosphere was treated as a single large well-mixed reservoir of such a size that the mid-1980's partial pressure of 348 ppm corresponded to an inventory of 750 GtC. At each timestep the atmospheric inventory was updated according to the fluxes to and from the ocean, and changes in atmospheric concentration were calculated as being proportional to the changes in inventory. In addition from model year 1286 onwards, CO_2 was continually added to the atmospheric reservoir at a constant rate of 5.4 GtC yr^{-1} to represent fossil fuel emissions. The rate at which CO_2 was added to the atmosphere is appropriate for the mid-1980's and the assumption of no increase in the rate corresponds to emission scenario D of the IPCC (1990) report. The purpose of this run was to look at the uptake of fossil fuel CO_2 by the ocean by comparing the results with those obtained at the end of the spin-up. The results, whilst not directly applicable to the present day uptake of CO_2, should give some idea of the proportion of anthropogenic CO_2 that the ocean can absorb and the time scale over which absorption occurs.

A further run was carried out, starting from the end of stage II of the spin-up at model year 1250, in which fossil fuel CO_2 was added to the atmospheric reservoir at the rate of 5.4 GtC yr^{-1} as before but this time annual mean forcing was used instead of seasonal forcing. This will be referred to as experiment B and was done in order to separate out the effects of seasonality. Note that experiments A and B start from different baseline carbon exchange figures, which needs to be taken account of in the comparison. Ideally, we would have liked to have run the model with constant CO_2 until the net flux had settled down to a figure below 0.1 GtC yr^{-1} for both simulations. However this would have required an excessive amount of computer time as the net carbon flux in the annual-mean run was decreasing at a very slow rate of 0.004 GtC yr^{-1} by year 1250.

Another run was performed in which spin-up stages I and II and experiment B were repeated, but with a smaller value of the background vertical diffusion coefficient (0.1 $cm^2\ s^{-1}$ instead of 0.5 $cm^2\ s^{-1}$). This is known as experiment C and a comparison with experiment B (which is otherwise identical) will reveal the influence of changing the vertical diffusivity.

All of the experiments described here were run in ocean-only mode. That is, atmospheric forcing is prescribed from climatology and is not allowed to respond to changes in the ocean model. Although the ultimate aim of this work is to provide us with an ocean carbon cycle model that can interact with and provide feedback to the atmosphere, we have chosen in the first instance to omit these feedbacks in order to keep the model as simple as possible. The development of the model in a coupled ocean-atmosphere context will be explored in future studies.

4. Results and discussion

4.1. The ocean circulation model

Before looking at the output from the carbon cycle model itself, it is instructive to examine some of the physical model output fields as these have a large effect on the CO_2 flux distributions to be seen later. Murphy (1994) provides additional discussion of the performance of an older, but essentially similar, version of the Hadley Centre model in the context of coupled modelling.

The total length of the spinup was 1250 years at the surface, and the equivalent of nearly 10,000 years in deep water, under annually-averaged forcing. A further 37 years was completed under seasonal forcing conditions. The portion of the run devoted to seasonal forcing was relatively short, the length of run being limited by computational expense. Complete adjustment of the deep ocean to the imposition of seasonal forcing is not possible, owing to the long timescales (on the order of centuries to millenia) associated with the deep circulation. However the surface layers of the ocean, which are arguably the most important on the timescale of these experiments, come into equilibrium quite rapidly. This is illustrated by Fig. 1 which shows the change in globally-averaged temperatures for selected layers over the entire period of seasonal forcing, normalised by the total change over the period. By the time the perturbation experiment commences, at model year 1287, the curves for the top 10 layers (300 m and above) have levelled off. Lower down, the curves show no sign of levelling out over the course of the run, indicating that the deep water is still some way from achieving a new equilibrium state. The maximum change in temperature occurs at 666 m, which cools at a rate of 0.24°C per century. At 1500 m the ocean warms by 0.074°C per century. The trends in absolute terms are thus quite small, and have little effect on the model's thermohaline circulation.

It is particularly important that a model that aims to simulate the uptake of gas from the atmosphere should represent ocean ventilation processes realistically and give a reasonable description of the formation of deep water. Figs. 2a and 2b show cross-sections of the annually-averaged zonal mean temperature for two runs of the model with different vertical diffusion coefficients, and Fig. 2c shows the observed distribution, taken from Levitus (1982). In the standard run (Fig. 2a) the model's thermocline is too deep and too diffuse. Also, the water just beneath the thermocline is too warm by as much as 3°C, most obviously south of the equator and in northern mid-latitudes. This results in the subpolar fronts being much steeper than observed. The model does at least manage to capture some of the features of the observed distribution quite well, particularly the vertically well-mixed region around 60°N and the north–south gradient in temperature in the southern hemisphere deep water. The low diffusivity run (Fig. 2b) is discussed in Subsection 4.3. Modelled

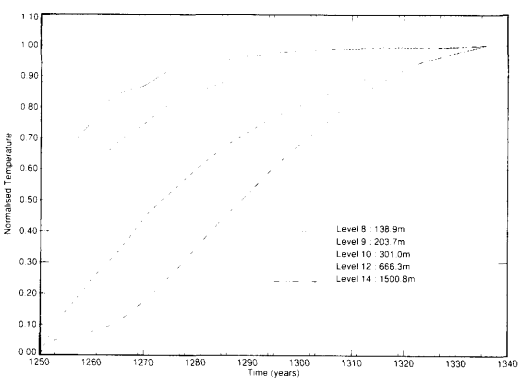

Fig. 1. Time variation of the normalised globally-averaged temperature during the seasonally-forced period of the run at levels 8, 9, 10, 12 and 14. Normalisation is calculated as $[T(t) - T_{\text{initial}}]/[T_{\text{final}} - T_{\text{initial}}]$.

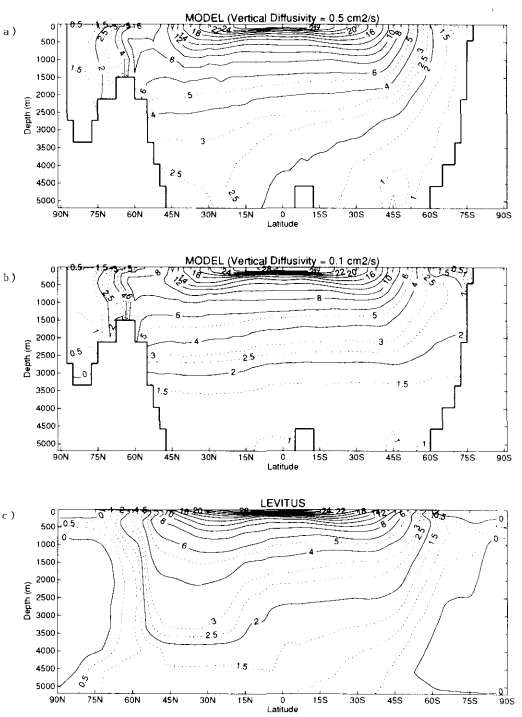

Fig. 2. Latitude-depth cross-sections of zonal-mean temperature (°C). (a) Standard run vertical diffusivity = 0.5 $\text{cm}^2\,\text{s}^{-1}$. (b) Vertical diffusivity = 0.1 $\text{cm}^2\,\text{s}^{-1}$. (c) Observed values from Levitus (1982). Contour interval is 0.5 below 3°C, 1.0 from 3°C to 6°C, and 2.0 above 6°C.

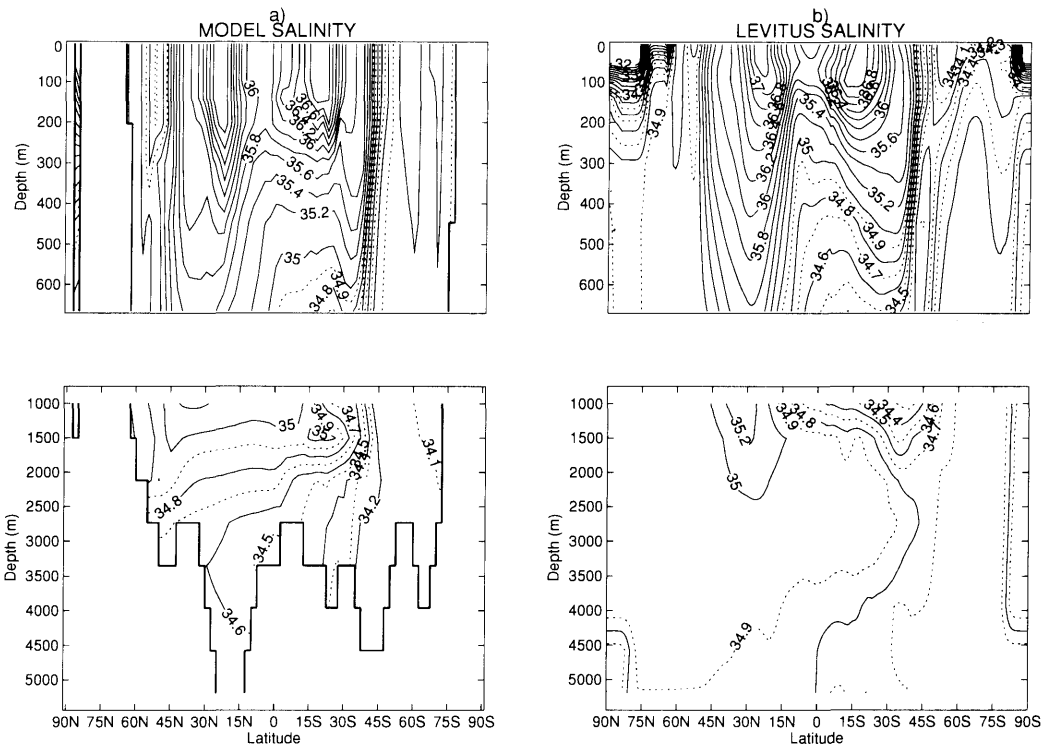

Fig. 3. Latitude-depth cross-section of Atlantic salinity (psu) at 37.5° W for (a) Model (standard run), and (b) observations (Levitus). Solid contours are at intervals of 0.2 psu. Dotted contours are at intervals of 0.1 psu below 35.0 psu.

and observed salinity sections through the Atlantic at 37.5° W are shown in Fig. 3. The model's source of antarctic bottom water (AABW) close to the coast of Antarctica, which should have a salinity of 34.7 psu, is too fresh by about 0.5 psu and this allows antarctic intermediate water (AAIW) of salinity around 34.5 psu to sink down to the bottom. The freshness of the model AABW is most likely due to the fact that the model's surface salinity is relaxed back towards the Levitus data, which is known to be too fresh close to Antarctica since the data is biased towards summertime values (England, 1992). Water of northern origin, such as North Atlantic Deep Water (NADW), which would normally occupy the bulk of the basin, has been restricted to depths shallower than 2500 m owing to its source water in the Norwegian Sea being too fresh and too warm during the long spin-up phase with annual-mean forcing. In the seasonally-forced part of the run the source water for NADW is produced only in the winter and its TS characteristics are thus more like those found in reality. Unfortunately a long spin-up run involving seasonal forcing, which would be necessary to give the correct salinity structure in the Atlantic, would be prohibitively expensive in computer time, since the techniques of split timestepping and deep-water acceleration may be inappropriate for non-steady forcing.

The model's simulation of the global water masses clearly leaves a lot to be desired. This appears to be a common feature among climate-resolution GCMs forced at the surface by annual mean climatology. The models of Toggweiler et al. (1989) and Maier-Reimer and Hasselmann (1987) have similar difficulties in reproducing the observed salinity and tracer patterns. More encouraging is the presence in this model of a tongue of fresher water at 1000 m in the southern hemisphere which extends as far north as the equator. This is intermediate water, and its appearance may be due to the fact that the

bathymetry across Drake Passage is quite realistic, in contrast to models of coarser resolution. England (1992) found that the adjustment of the bathymetry of Drake Passage in a coarse resolution model, so that the tip of South America presented more of a barrier to circumpolar flow, resulted in a weakening of the wind-driven Deacon cell and an improvement in the northward penetration of AAIW.

As well as temperature and salinity sections, we also present the distributions of natural (i.e., pre-bomb) radiocarbon computed by the model. Fig. 4 shows a map of surface values. Highest $\Delta^{14}C$ values are found in the subtropics, reflecting the longer times for which water is at the surface. The lowest values are close to the coast of Antartica, where $\Delta^{14}C$ reaches $-90‰$, some $10‰$ higher than estimates of the surface pre-industrial concentrations given by Broecker and Peng (1982). The average value over the region 30°N to 30°S is $-40‰$, in excellent agreement with estimates made by Toggweiler et al. (1989) based on coral measurements. Fig. 5 shows meridional sections through the Atlantic and Western Pacific oceans. The Pacific has the oldest waters with lowest ^{14}C concentrations of $-240‰$ on the bottom at 45°N. The ^{14}C concentrations are comparable to those found in the Geosecs data (Broecker and Peng, 1982), but in the data the minimum occurs at about 2500 m rather than on the bottom. The model captures the north–south slope of isolines in the deep water of the northern hemisphere which is seen in observations, but the deep water up against the coast of Antarctica has ^{14}C concentrations which are too high ($100‰$, as compared with $160‰$ seen in the observations) suggesting that

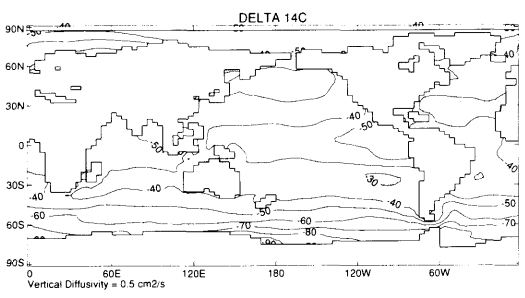

Fig. 4. Predicted $\Delta^{14}C$ ($‰$) at the surface from the standard run of the model. Contours are drawn at intervals of $10‰$. Values above $-30‰$ are shaded.

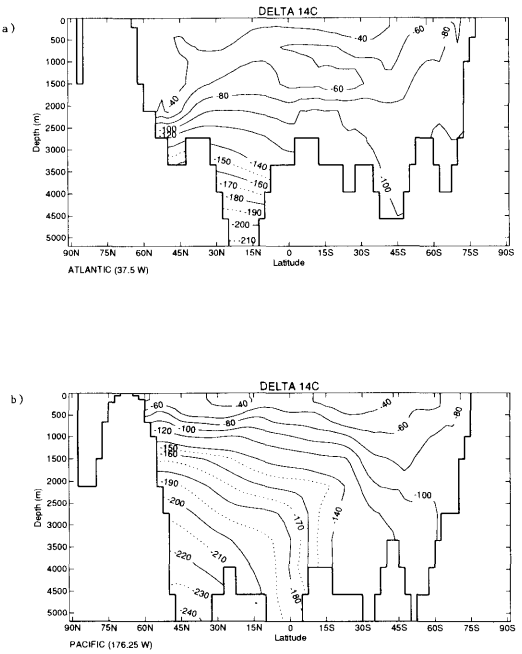

Fig. 5. Predicted latitude-depth cross-sections of $\Delta^{14}C$ ($‰$) from the standard run through (a) the Atlantic at 37.5°W, and (b) the Pacific at 176.25°W. Solid contours are drawn at intervals of $20‰$. Dotted contours are at intervals of $10‰$ below $-150‰$.

the ventilation in this region may be too strong. Although the Pacific compares quite well with observations, the simulation in the Atlantic is less good. The ^{14}C concentration in the deepest part of the basin is too low by some $50‰$ (cf. Broecker and Peng, 1982, Fig. 5.5). The model produces North Atlantic deep water of the correct ^{14}C concentration (about $-80‰$), but it is unable to sink below 2500 m, resulting in insufficient ventilation of the bottom water in the northern hemisphere. This same feature is seen in the salinity section shown in Fig. 3a. In general, though, the model gives a reasonable simulation of the radiocarbon distribution. The model results resemble those obtained by Toggweiler et al. (1989) in their experiment C, which were obtained using a relatively high diffusivity of 1.0 $cm^2\ s^{-1}$.

The model predicts a Gulf stream transport of 38 Sv, similar to that observed (Knauss, 1969), and an Antarctic Circumpolar Current of strength 130 Sv, again close to observations (Nowlin and Klinck, 1986). Depth-mean flow through the

Indonesian Passage is allowed in the model, and its predicted strength is 24 Sv, which is somewhat larger than the estimate of 16 Sv given by the Sverdrup model of Godfrey (1989). One possible reason for this may be that the Indonesian sill, at 1200 m, is too shallow, causing strong cross-sill pressure gradients to be set up (Hirst and Godfrey, 1993). The peak poleward heat transport is 0.99 Petawatts at 32.5° N. This is lower than recent estimates of 3.75 and 1.5 Petawatts (Carrissimo et al., 1985; Hsuing, 1985), but is comparable to other models (e.g., Bryan and Lewis, 1979).

To summarise this section, whilst the modelled circulation characteristics appear reasonable, there are a number of areas where improvements are desirable. The deficiencies of the model highlighted in this section should be borne in mind when examining the uptake of gases.

4.2. The carbon cycle model with seasonal forcing

We first of all look at the results from the steady state carbon cycle at the end of the seasonal spin-up run (stage III) before examining the model's uptake of anthropogenic CO_2.

4.2.1. The steady-state carbon cycle. Fig. 6 shows the surface T_{CO_2} in μmol kg^{-1} at the end of the spinup (following the application of seasonal forcing). This plot is strongly related to the annual mean sea surface temperature pattern (not shown) with lowest carbon concentrations in the warm waters of the tropics and higher values in the cold waters of high latitudes. A tongue of higher T_{CO_2} values is evident in the tropical east and central Pacific. There is very little variation in T_{CO_2} in the model throughout the year, despite the strong seasonality of the SST field. The T_{CO_2} pattern is essentially controlled by the long-term pattern of SST - at higher temperatures the partial pressure of CO_2 is higher, resulting in the loss of CO_2 to the atmosphere. Conversely, in cold water gas solubility is greater and the partial pressure is lower, encouraging the invasion of CO_2 from the atmosphere and thus higher concentrations. The air-sea gas exchange rate for CO_2 is slow (the equilibration time for CO_2 is of the order of 1 year), and thus seasonal changes in T_{CO_2} caused by interaction with the atmosphere are slight. This absence of seasonality in T_{CO_2} is in contrast to reality, where changes in T_{CO_2} of order 100 μmol kg^{-1} can be observed, with lowest values in summer and highest values in winter caused by transport of deep water to the surface due to mixing (Takahashi et al., 1993). The model's seasonal variation does not exceed 5 μmol kg^{-1}. Fig. 7 shows a zonally averaged vertical cross-section of the modelled T_{CO_2} distribution. Whilst the surface values are well simulated, the deep ocean values are far too low. Deep water T_{CO_2} as high as 2400 μmol kg^{-1} are observed in the oldest water of the Pacific. There is also no hint of the observed mid-depth maximum in equatorial waters at about 1000 m. This deficiency is attributable to the neglect of ocean biology which tends to pass carbon rapidly from the surface in the form of sinking particles. Remineralisation of these particles increases the deep-water T_{CO_2} and is responsible for the mid-depth maximum. The oldest waters have highest values of T_{CO_2} since they have had more time to receive particles falling from the surface. Given the model's low deep water T_{CO_2} concentration, we might expect our surface values of T_{CO_2} to be too low in regions of strong upwelling and deep mixing. This results in the suppressed seasonal cycle in the model's surface T_{CO_2}. The other effect of biology is to cause a sharp

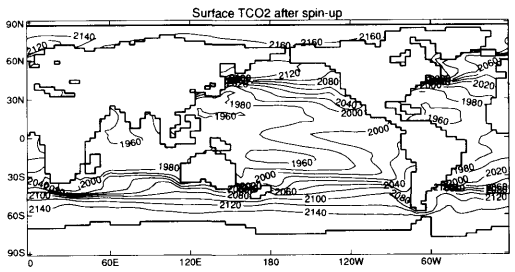

Fig. 6. Annual mean surface T_{CO_2} (in μmol kg^{-1}) at the end of the spin-up run. Contour interval is 20 μmol kg^{-1}.

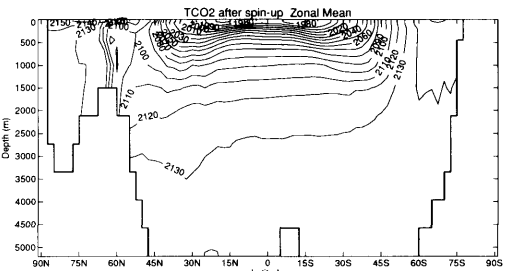

Fig. 7. Zonally-averaged meridional section of T_{CO_2} (in μmol kg^{-1}) at the end of the spin-up run. Contour interval is 10 μmol kg^{-1}.

decrease in T_{CO_2} in the North Atlantic during spring and summer due to the spring bloom. This mechanism, absent from the model, also reduces the seasonal response.

The difference between the sea surface partial pressure of CO_2 and the atmospheric partial pressure of 348 ppm is plotted in Fig. 8 for January–March and July–September. Regions where the oceanic partial pressure is lower than the atmospheric value, and CO_2 is liable to enter the ocean, are shaded. Oceanic pCO_2 is greater than the atmospheric value in low latitudes, and lower in middle and high latitudes. The oceanic excess reaches values of between 60 and 80 ppm in the tropics and sub-tropics. Much of the middle latitudes show a deficit of 20 to 40 ppm whilst there are two regions of rather intense deficit as high as 80 ppm to be found in the North West Atlantic and North West Pacific, north of the Gulf Stream and Kuroshio currents during winter and spring. Lowest partial pressures are found around the coast of Antarctica and in the Arctic ocean, where deficits greater than 60 ppm are common,

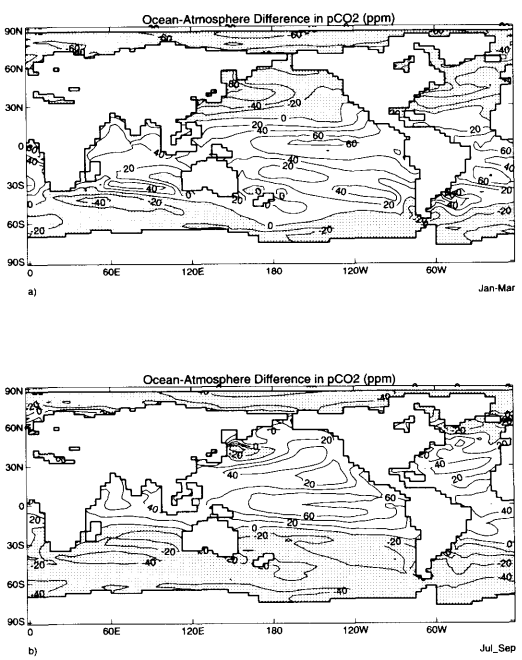

Fig. 8. Model ΔpCO_2 in ppm at the end of the spin-up run for (a) January to March; and (b) July to September. Contour interval is 20 ppm. Negative values (representing gas flux into the sea) are shaded.

and values up to 120 ppm below the atmospheric value can be found during winter (not apparent from the plots). There is broad agreement between the modelled pCO_2 differences and those observed over the period 1972–1989 (Tans et al., 1990, Fig. 3), given the sparseness of the observations on which the data are based and taking into account the fact that the model values and observations represent slightly different times of year. However, a comparison of the model with more detailed seasonal data obtained over the past decade in the North and South Atlantic and North Pacific oceans (Takahashi et al., 1993) reveals a number of discrepancies which can be attributed to the lack of biology in this model. These data show high partial pressures in high latitudes during winter, with lower values in summer and a steep fall in partial pressure in the North Atlantic at the time of the spring phytoplankton bloom. The higher winter values are associated with upwelling of deep waters rich in CO_2. In the model, on the other hand, the lowest partial pressures occur in winter at high latitudes, since variations in pCO_2 are dominated by sea surface temperature changes - winter upwelling of deep water has little effect on the model pCO_2 since the amount of CO_2 in deep water is too low. Owing to the neglect of biology, therefore, the seasonal cycle of model pCO_2 is of opposite phase to that seen in reality. Whether or not this failure of the model has a significant effect on uptake of excess anthropogenic CO_2 from the atmosphere remains to be seen. It may be that the seasonal variation of pCO_2 at a particular location is of little significance provided the annual average pCO_2 is correct. On the other hand, lower partial pressures during winter may favour a stronger flux of excess CO_2 into the ocean during that season due to stronger vertical mixing at that time of year. This is an issue that will be resolved once biology is introduced into the model.

Fig. 9 shows the gas flux between atmosphere and ocean. The gas flux is governed mainly by the difference in partial pressures between atmosphere and ocean, but is also dependent on wind speed according to the Liss and Merlivat formula (eq. (9)). Thus CO_2 leaves the ocean in the tropics and subtropics at a rate of up to 2 mol m^{-2} yr^{-1} and invades the ocean in the North Atlantic, the North Pacific and the Southern and Arctic oceans. Intense regions of strong invasion (up to 7 mol m^{-2} yr^{-1}) are found in winter in the North West

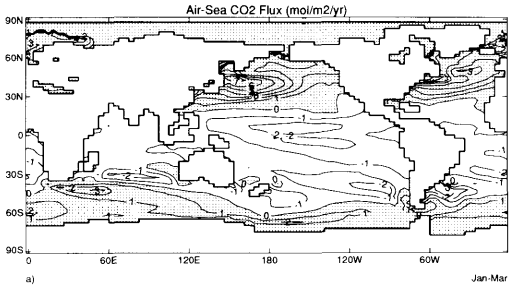

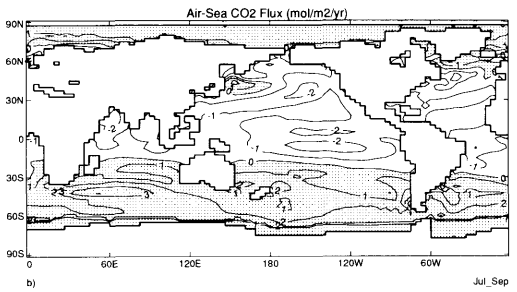

Fig. 9. Atmosphere-ocean gas flux in mol m^{-2} yr^{-1} during the latter stages of the spin-up. (a) January to March. (b) July to September. Contour interval is 1 mol m^{-2} yr^{-1}. Positive values, representing flux into the ocean, are shaded.

Atlantic and Pacific where the strong winds in the path of the mid-latitude storm tracks amplify the effect of the peaks in air-sea pCO_2 difference found there. Although less intense, the Southern Ocean appears to be an important sink owing to the large area over which CO_2 is entering the ocean, particularly in the Indian Ocean sector where the wintertime mixing extends down to around 500 m. Notice also that although by far the lowest values of oceanic pCO_2 were found in the Arctic ocean and immediately adjacent to the coasts of Antarctica, very little exchange with the atmosphere occurs in those regions as the sea is covered in ice and the CO_2 can only invade the ocean through leads and polynyas in the ice. A very strong seasonal variation is evident, as can be seen from a time-latitude plot of the zonally averaged flux (Fig. 10). The seasonality is much stronger in the northern hemisphere than in the south with the largest peak values occurring at 45° N. The intense

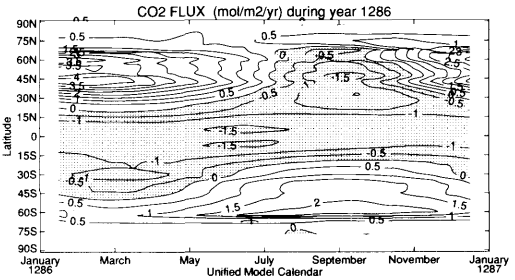

Fig. 10. Time-latitude plot of the zonal mean CO_2 flux in mol m^{-2} yr^{-1} during the final year of the spin-up. Contour interval is 0.5 mol m^{-2} yr^{-1}. Negative values, representing flux out of the ocean, are shaded.

atmosphere-to-ocean flux which occurs in late winter and early spring at 45° N is offset by a flux out of the sea in the same region during late summer and early autumn. The equatorial region remains a source to the atmosphere throughout the year, the southern-most part of the Southern Ocean and the extreme North Atlantic and Arctic ocean are sinks throughout the year, whilst much of the mid-latitudes can act as either a source or a sink for CO_2 depending on season. In particular, much of the North West Pacific, which has the strongest uptake of any region during winter, acts as a weak source during the summer months. Outgassing from the ocean can occur as far north as 70° N, whilst the southern hemisphere acts as a sink throughout the year south of 50° S. Over the whole globe the net air-sea flux is close to zero (less than 0.05 GtC yr^{-1}).

4.2.2. Uptake of anthropogenic CO_2. We turn now to experiment A and the uptake of anthropogenic CO_2 by the model ocean. Fig. 11 shows the globally-averaged net flux of CO_2 from the atmosphere into the ocean during the seasonally forced part of the integration. The seasonal cycle has been removed from this figure by averaging over a period of a year. Until year 1286 the net flux is less than 0.05 GtC yr^{-1}, at which point CO_2 is added to the well-mixed atmospheric box at a rate of 5.4 GtC each year. There is an initially rapid rise in the carbon flux into the ocean over the next 10 or so years, which begins to level out. By year 1336, after 50 years of CO_2 being added to the atmosphere, the net flux is 2.4 GtC yr^{-1}. At this point, the net flux is rising at a rate of just 0.007 GtC yr^{-1}. Over a 50-year period, then, the ocean has adjusted to the extra

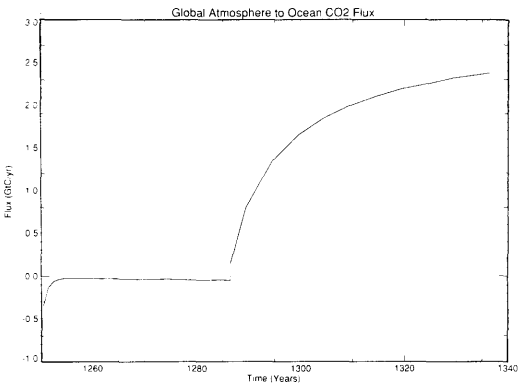

Fig. 11. Time series of the global net exchange of carbon in GtC yr^{-1} between atmosphere and ocean during stage III of the spin-up and experiment A, the seasonally forced part of the integration. After year 1286 CO_2 was added to the atmosphere at a constant rate of 5.4 GtC yr^{-1}. The seasonal cycle has been suppressed in the figure by plotting annual mean fluxes.

CO_2 emissions so that it is taking up 44% of the annual output - an airborne fraction of 0.56. Our results support the high uptake figures obtained with other ocean models, indeed this model predicts a slightly higher uptake than those reported previously (Maier-Reimer and Hasselmann, 1987; Sarmiento et al., 1992). Our results suggest that, given enough time to adjust to the anthropogenic emission scenario, the ocean is capable of absorbing greater than 40% of anthropogenic carbon if the influence of biological effects on the basic carbon cycle climatology is omitted.

There is, as one might expect, substantial temporal and spatial variation in the uptake of anthropogenic CO_2 simulated by the model. Fig. 12 shows maps of the air-sea flux of excess CO_2 after 50 years of experiment A averaged over two 3-month periods: January–March and July–September. The zonally averaged Hovmuller plot of the same quantity is plotted as Fig. 13. Excess CO_2 flux is calculated as the difference between the fluxes obtained during experiment A and those obtained at the end of the spin-up, before extra CO_2 was added to the atmosphere. The maps are therefore a direct measure of where the atmospheric CO_2 is entering the ocean. The strongest uptake of "anthropogenic" CO_2 takes place at 45° N on the western sides of the North

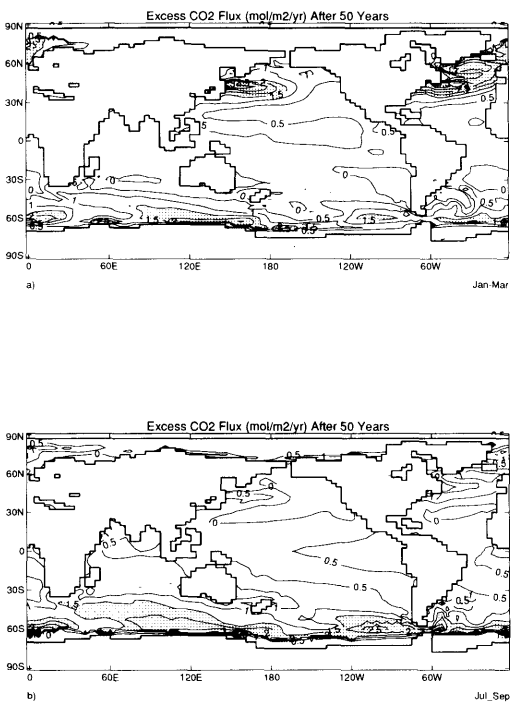

Fig. 12. Atmosphere to ocean flux of excess CO_2 in mol m^{-2} yr^{-1} after 50 years of experiment A for (a) January to March, and (b) July to September. Contour interval is 0.5 mol m^{-2} yr^{-1}. Fluxes in excess of 1.5 mol m^{-2} yr^{-1} are shaded. Excess CO_2 flux was obtained by plotting the difference between the fluxes during experiment A and those at the end of the spin-up run.

Atlantic and North Pacific, and immediately south of Greenland and Iceland as well as in the Nordic Seas. Fluxes as high as 4 mol m^{-2} yr^{-1} are attained. However, these fluxes are highly seasonal, and the northern hemisphere contributes very little in the absorption of excess atmospheric CO_2 between May and September (Fig. 13). In the southern hemisphere, peak values are generally lower (except for some isolated areas of high flux adjacent to the ice edge during the austral winter which are an artifact caused by interannual variations in the exact location of the ice edge and the method used of obtaining the excess flux by differencing). However, a significant flux in excess of 0.75 mol m^{-2} yr^{-1} occurs throughout the year at all latitudes between 50° S and the ice edge. Excess CO_2 uptake in gigatonnes of carbon per year summed over various regions of the world ocean are given in Table 3 for northern hemisphere

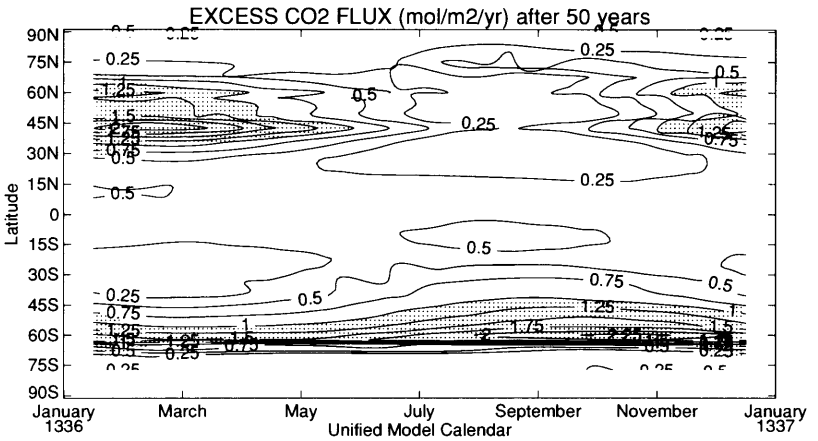

Fig. 13. Time-latitude plot of the zonal mean excess CO_2 flux in mol m^{-2} yr^{-1} after 50 years of experiment A. Contour interval is 0.25 mol m^{-2} yr^{-1}. Fluxes in excess of 1 mol m^{-2} yr^{-1} are shaded. Excess CO_2 flux was obtained by plotting the difference between the fluxes during experiment A and those at the end of the spin-up run.

winter and summer, and for the annual mean. Averaged over the year, the three northern regions (N. Pacific, Atlantic Gyre and Atlantic Subarctic) account for roughly equal amounts of carbon, totalling 0.69 GtC yr^{-1} between them. The equatorial region, extending from 15°N to 15°S, accounts for 0.5 GtC yr^{-1}. This is at first sight rather surprising as the tropics is often thought of as a source region for CO_2 (see Figs. 9, 10). However, it simply means that when the extra CO_2 is added to the atmosphere, the equatorial oceans are releasing less CO_2 back to the atmosphere than before due to the reduced partial pressure difference between atmosphere and ocean. The largest sink for anthropogenic CO_2 according to this model occurs in the southern hemisphere where the Southern Gyres and Antarctic regions take up 0.7 and 0.6 GtC yr^{-1} respectively. The area south of 15°S thus accounts for 54% of the total uptake of excess CO_2, whilst the tropics contributes a further 21% of the total. These figures are in broad agreement with the perturbation

Table 3. *Oceanic uptake of excess CO_2 after 50 years of emissions*

Region	January to April	July to October	Annual mean
Atlantic subarctic >50°N; 90°W to 20°E	0.3	0.1	0.2
Atlantic gyre 15°N to 50°N; 90°W to 20°E	0.4	0.1	0.2
north Pacific >15°N; 110°E to 90°W	0.4	0.0	0.2
equatorial 15°S to 15°N; 180°W to 180°E	0.5	0.6	0.5
southern gyres 50°S to 15°S; 180°W to 180°E	0.3	1.0	0.7
antarctic >50°S	0.5	0.7	0.6
global	2.4	2.5	2.4

uptake simulation of Sarmiento et al. (1992) although in their model the equatorial region takes up slightly more CO_2 (28%).

A comparison of CO_2 uptake between the Tans et al. (1990) analysis and the present model is presented in Table 4. It is difficult to compare our model with the Tans et al. (1990) figures directly, since we are looking at the response of the ocean to CO_2 added at a constant rate, whereas the Tans et al. (1990) model is attempting to simulate the flux at a particular time in history. However, since our model's annually-averaged global uptake varies from zero to 2.4 GtC yr^{-1} over the course of the experiment, by choosing the moment when our uptake matches the Tans et al. (1990) figure of 1.6 GtC yr^{-1}, and comparing the two models at this stage when the global figures are equal, we can concentrate on looking at differences in location and timing of CO_2 uptake. Table 4 gives the gross fluxes of carbon, inclusive of the undisturbed, "pre-anthropogenic", fluxes before the addition of extra CO_2. There are considerable differences between our model and the Tans et al. (1990) estimates of the annual uptake. Tans et al. (1990) estimate that the southern gyres take up a massive 2.39 GtC yr^{-1}, whilst the model gives just 0.79 GtC yr^{-1} with a further contribution of 0.96 GtC yr^{-1} from the region around Antarctica. In the model the northern hemisphere assumes more importance in relation to the southern hemisphere compared with the Tans et al. (1990) estimates, absorbing about 70% of the southern hemisphere total. The model's equatorial region emits about 30% less CO_2 than the Tans et al. (1990) estimate. The model also exhibits greater seasonal variation than the estimates. We do not support the high uptake of the southern gyres given by the observationally-based estimate. This is in accordance with atmospheric transport modelling studies by Tans et al. (1990) and Keeling et al. (1989). However, we do predict a fairly large sink of order 1 GtC yr^{-1} south of 50° S. Close agreement with the estimates in the tables for the southern hemisphere is perhaps not to be expected owing to the sparseness of data in the South Pacific, South Indian and Southern Oceans, particularly in the southern winter. The northern hemisphere is much better sampled and we would expect the data to be better constrained there. However, here there may be substantial time variations in partial pressure which may not be well captured by the data. In particular, phytoplankton blooms may lower partial pressures by as much as 100 ppm during spring and summer, resulting in enhanced uptake by the ocean (or reduced evasion to the atmosphere). This process is not yet included in the model. It would tend to increase the modelled uptake during July to October providing better agreement with observations for this period. From January to April the northern hemisphere sink is much stronger than is suggested by the observations, particularly for the North Pacific. Again, the inclusion of biological processes would tend to bring the modelled uptake closer to the data-based estimates, through the increase in partial pressure caused by bringing up high-T_{CO_2} water from depth. Thus the inclusion of biology might be expected to bring seasonal variations in the modelled fluxes into closer alignment with observations without necessarily affecting the net uptake of anthropogenic CO_2. Over the year the model's combined northern hemisphere sink

Table 4. *Atmosphere-ocean CO_2 flux: comparison of model with observationally-based estimates of Tans et al. (1990)*

Region	January to April		July to October		Annual mean	
	model	Tans	model	Tans	model	Tans
Atlantic subarctic	0.89	0.15	0.07	0.31	0.51	0.23
Atlantic gyre	0.80	0.58	−0.23	0.02	0.23	0.30
north Pacific	1.28	0.44	−0.43	−0.33	0.46	0.06
equatorial	−1.15	−1.56	−1.10	−1.69	−1.17	−1.62
southern gyres	−0.47	1.46	1.99	3.31	0.79	2.39
antarctic	0.64	0.38	1.26	0.03	0.96	0.20
global	1.56	1.5	1.55	1.7	1.59	1.6

strength is 1.2 GtC yr^{-1}, which is of comparable magnitude to the southern hemisphere value of 1.75 GtC yr^{-1} and the equatorial source of 1.2 GtC yr^{-1}.

Fig. 14 compares the response of the various regions identified in Table 3 to the increase in atmospheric pCO_2. In the period immediately prior to model year 1286, the point at which atmospheric CO_2 concentrations started to increase, the Atlantic Subarctic, North Pacific and Antarctic regions are still adjusting to the change from annual mean to seasonal forcing which occurred at year 1250. This may be related to a change in high latitude convection characteristics and a greater influence of NADW on the global scale water masses under seasonal forcing conditions. Prior to year 1286 the largest portion (just over 40%) of the CO_2 emitted from the tropics is absorbed by the Antarctic region. The Atlantic Subarctic takes up 23% and the North Pacific and Southern Gyres each contribute about 16%. After year 1286 the Southern Gyres region shows an initially rapid rise in air-to-sea flux, but the uptake curve saturates after about 25 years, by which time this region is absorbing 12% of the excess CO_2 added to the atmosphere each year. The 3 northern hemisphere regions show more modest rises with each region contributing approximately equally to the combined northern uptake. A slight trend is still evident in each northern region at the end of the run. The Antarctic, south of 50°S, initially takes up carbon at a slower rate than its neighbouring area to the north, but unlike the Southern Gyres does not reach a plateau. By the end of 50 years, this area accounts for 12% of the "anthropogenic emissions" and the curve is still rising at a rate of 0.005 GtC yr^{-1}. The equatorial region also absorbs a significant proportion of the emissions and shows a rising trend of 0.003 GtC yr^{-1}. The regions with the longest response time to an atmospheric CO_2 increase are, as one might expect, those regions where deep water is being brought up to the surface to replenish water saturated with excess CO_2.

The plots shown thus far depict the movement of carbon into the surface of the ocean, but what happens to that CO_2 once it is absorbed in the mixed layer? Fig. 15 shows meridional sections through the Pacific and Atlantic oceans of the excess CO_2 from experiment A. After 50 years the anthropogenic CO_2 has not penetrated below 1000 m in the tropical Atlantic ocean, but north of 35°N and south of 35°S the anthropogenic signal has reached the bottom of the ocean. The deep North Atlantic in particular shows a significant

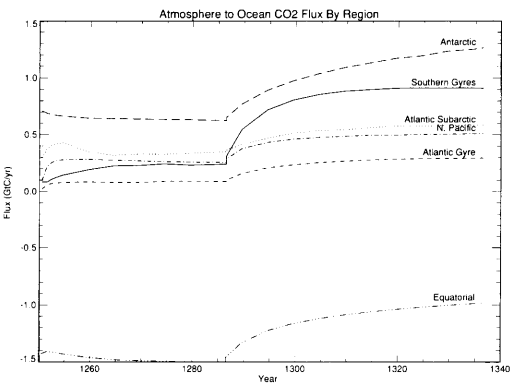

Fig. 14. Time-series of atmosphere to ocean CO_2 flux (in GtC yr^{-1}) for each of the regions defined in Table 3 for stage III of the spin-up and experiment A, the seasonally forced part of the integration. The seasonal cycle has been suppressed in the figure by plotting annual mean fluxes.

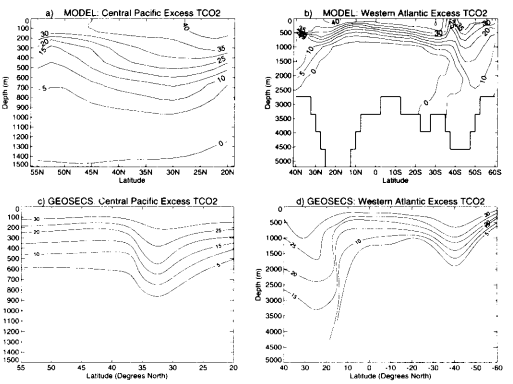

Fig. 15. (a, b) Meridional sections of excess T_{CO_2} in μmol kg^{-1} after 50 years of experiment A for (a) the North Pacific ocean at 150°W, and (b) the Atlantic ocean at 37.5°W. Excess T_{CO_2} is obtained by plotting the difference between T_{CO_2} during experiment A, and at the end of the spin-up run. Contour interval is 5 μmol kg^{-1}. (c, d) Observationally-based estimates of excess T_{CO_2} from the GEOSECS expedition for (c) the North Pacific ocean (redrawn from Chen, 1982b), and (d) the western Atlantic ocean (redrawn from Chen, 1982a). Contour interval is 5 μmol kg^{-1}.

Tellus B/47/1/2-11

increase in T_{CO_2} of 20 μmol kg^{-1} in water as deep as 2000 m (at 50°N, off the plot). The highest increase in T_{CO_2} of up to 40 μmol kg^{-1} occurs in the subtropical gyres above the thermocline and the typical bowl-shape of the thermocline beneath the subtropical gyres can be clearly seen. In the Indian and Pacific oceans anthropogenic CO_2 again reaches the ocean bottom in the Southern hemisphere. Excess CO_2 can be seen as deep as 1500 m in the equatorial Pacific. Anthropogenic CO_2 is taken up into deep water in the North Atlantic (through the formation of NADW) and throughout the Southern Ocean (in AABW and AIW formation). The greater intensity of NADW formation results in fairly high deep water concentrations in the northern north Atlantic but the area over which this occurs is necessarily rather small. The southern hemisphere deep water formation simulated by the model occurs over a much wider area and there is a very large volume of water which is available to absorb the excess CO_2. The southern hemisphere thus acts as a larger sink for anthropogenic CO_2 than the northern hemisphere in this model. A rough check on the plausibility of the model can be made by comparing the results with observationally-based estimates of excess T_{CO_2} provided by Chen (1982a, 1982b). These estimates for a central Pacific section and the Atlantic Geosecs section are also shown in Fig. 15. The comparison with the model is not exact since the model shows the response to 50 years of emissions at a constant rate of 5.4 GtC yr^{-1}, whilst the data reflects emissions rising over a period of almost 200 years from zero to 5.4 GtC yr^{-1}. The cumulative release of CO_2 from fossil fuel use from 1850 to 1987 is estimated at 200 GtC (Marland, 1989), as compared with a total output of 270 GtC in the model. We can however compare the general shape of the sections. There is reasonably good agreement. Comparison of Fig. 15b with Fig. 15d shows that the model's T_{CO_2} penetration is slightly overstrong in the Southern Ocean and that the T_{CO_2} originating in the North Atlantic does not extend as far south along the bottom as is observed. The reasons for this were discussed in Subsection 4.1. Maier-Reimer and Hasselmann (1987) have greater penetration of excess T_{CO_2} in the South Atlantic in their model, whilst the Sarmiento et al. (1992) model shows very little. The behaviour of this model appears to lie somewhere between the two. In the North Pacific both the penetration and structure of the model results agree fairly well with the observations, indicating that the thermocline ventilation characteristics of the model are approximately correct.

4.3. *Annual-mean forcing: comparison with seasonal forcing*

The carbon cycle simulations reported thus far in the literature describe results obtained using annual-mean forcing. One of the purposes of this work was to examine the effects on CO_2 uptake of including seasonal variations. The previous sections showed the large variations throughout the year of pCO_2, ice cover and mixed layer depth. Gas exchange coefficient also undergoes marked seasonal variation through its dependence on the wind speed via the Liss and Merlivat formula (eq. (9)). In mid-latitudes the winds are much stronger in winter than in summer which results in a larger gas exchange coefficient and a deeper mixed layer, resulting in a larger reservoir available for absorbing CO_2. pCO_2 is also lower in winter because of lower SSTs. Thus the flux into the ocean in winter when ΔpCO_2 is positive should be stronger than the summertime flux out of the ocean when ΔpCO_2 is negative. One might expect, therefore, the results from simulations that include the seasonal cycle to be somewhat different from those from a model forced with annually-averaged fields. To test this out, we performed a simulation, parallel to experiment A, in which atmospheric CO_2 is increased at the same rate as before, but the model is forced with an annually-averaged version of the climatology used to force experiment A. This annual-mean simulation is referred to as experiment B. Apart from their forcing, experiments A and B are otherwise identical. It is not quite as straightforward as one might wish to compare experiments A and B because they were started from different baselines. Experiment A was started from the seasonal stage of the spin-up at which time the global net CO_2 flux between atmosphere and ocean was 0.04 GtC yr^{-1} out of the ocean. Experiment B started from the annually-forced stage of the spin-up at which time there was a flux out of the ocean of 0.35 GtC yr^{-1}. Allowance has been made for the different starting points of the two experiments.

Fig. 16 shows the atmosphere-ocean flux for the 50 years during which the seasonally- and annual-mean-forced experiments were run. The curves

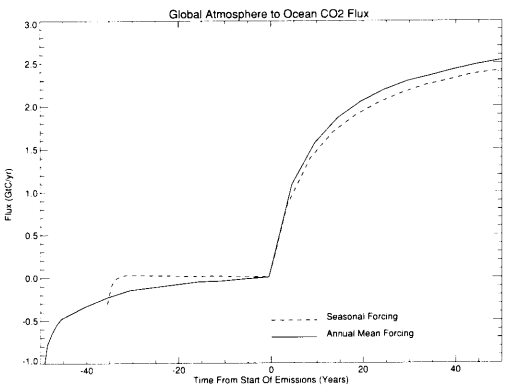

Fig. 16. Comparison between global atmosphere-to-ocean CO_2 flux under conditions of annual-mean forcing and seasonal forcing. Each curve has been plotted so that it starts from an initial flux of zero at the time emissions to the atmosphere started.

have been offset so that they both start from an initial flux of zero GtC yr^{-1}. After 5 years, the curves start to diverge, but after 50 years the model takes up excess atmospheric carbon at a rate of 2.42 GtC yr^{-1} in the seasonally forced case compared with 2.53 GtC yr^{-1} in the annual-mean run, a difference of only 0.1 GtC yr^{-1}. One could, however, object to this interpretation on the grounds that the two stages of the spin-up immediately prior to the start of experiments A and B exhibit quite different trends, as can be seen from Fig. 16. For the seasonal spin-up the atmosphere-ocean flux is decreasing at a rate of 0.001 GtC yr^{-1} whilst in the annual-mean spin-up the flux is increasing at 0.004 GtC yr^{-1}. If these trends are removed from the curves of Fig. 16 then the seasonally-forced model appears to be taking up carbon at a rate of 0.1 GtC yr^{-1} greater than in the annual-mean case. Whichever way we look at it, the use of annual mean as opposed to seasonal forcing has remarkably little effect on the global uptake of carbon by the ocean. By the end of 50 years of emissions, the difference between the two runs is 0.1 GtC yr^{-1}, just 4% difference. We therefore conclude that, contrary to expectations, the inclusion of a seasonal cycle has little effect on the annual-mean, global uptake of CO_2. This seems somewhat surprising in view of the discussion above and the effect of seasonally varying ice cover and SSTs on North Atlantic Deep Water formation. The small influence of seasonality can perhaps be explained by the predominance of the southern hemisphere and the tropics in the absorption of excess CO_2 (Fig. 14) combined with the effects of seasonality being confined more to the northern hemisphere as can be seen from Fig. 13. The fluxes south of 30°N show relatively minor variations through the seasons.

4.4. The effect of changing the diffusivity

Bryan (1987) showed, in a series of experiments using simplified GCMs, that the thermohaline circulation of such models is very sensitive to the value used for the coefficient of vertical diffusivity. Higher diffusivity results in a thicker thermocline which causes stronger north–south pressure gradients to be set up at the depth of the thermocline, and this drives a stronger meridional circulation. The values of diffusivity typically used range from 0.1 $cm^2 s^{-1}$ to 1.3 $cm^2 s^{-1}$. The lower value tends to keep the thermocline thickness close to observations but results in a meridional circulation that is too sluggish. The higher value has a more realistic overturning but too diffuse a thermocline. In practice the value actually used tends to be based on a compromise between these two effects. What is represented as diffusion corresponds in the real ocean to a variety of processes, such as mixing by breaking internal waves, double diffusion, thermohaline staircases and so on. The dominant process varies from region to region as well as in time and so the use of a constant diffusion coefficient is a very crude parameterization. The same coefficient tends to be used for heat and salt, with little justification. Gargett and Holloway (1992) showed that models such as these are also sensitive to the relative magnitudes of heat and salt diffusivities if separate coefficients are used. Unfortunately it seems that some parts of the ocean will have stronger heat diffusion, whilst others will have stronger diffusion of salt depending on whichever physical process is dominant at any particular time. This makes the problem of parameterization even more acute.

In order to assess the impact on CO_2 uptake of poor knowledge of the vertical diffusion coefficient we performed another experiment, parallel to experiment B, in which the background vertical diffusivity of heat, salt and T_{CO_2} was reduced from 0.5 $cm^2 s^{-1}$ to 0.1 $cm^2 s^{-1}$. All other aspects of the two experiments were identical. The run with the lower diffusion coefficient is referred to as experi-

ment C. Both diffusivities are plausible values, lying at the mid- and low-ends of the commonly-used range of values. The meridional volume transport for the global ocean for each experiment is shown in Fig. 17. The wind-driven surface cells in the tropics and the two sub-surface cells have declined in strength by between 20 and 30% as the diffusivity has been decreased. The southerly Ekman cell is 500 m shallower than before and the convective cell close to the coast of Antarctica has been lost. The Deacon cell centred at 45°S has changed little in maximum strength, and the deep cell centred at 15°S is much less vigorous than before. Meridional sections of the zonally averaged excess T_{CO_2} after 50 years of emissions are shown for the two experiments in Fig. 18. For the higher diffusivity case, the thermocline is thicker and the 10 μmol kg^{-1} isoline is some 100 m deeper in the tropics. The thermocline is less "bowl-shaped" in

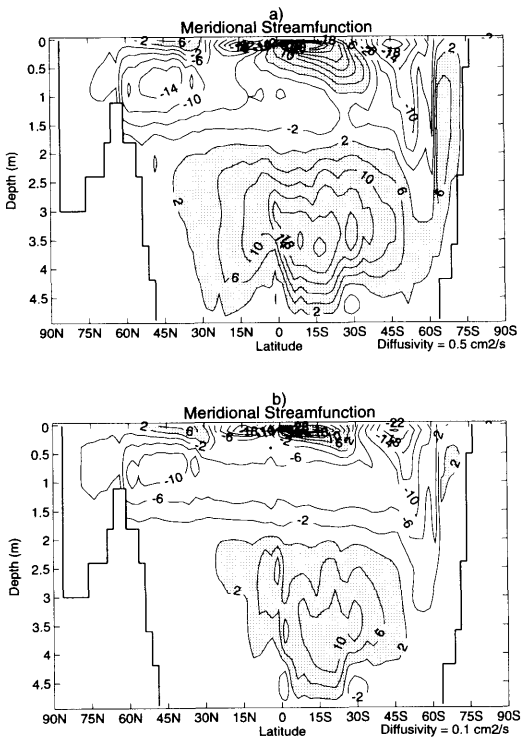

Fig. 17. Global meridional overturning circulation for annual-mean forcing with background vertical diffusivities of (a) 0.5 cm^2 s^{-1}, and (b) 0.1 cm^2 s^{-1}. Contour interval is 4 Sv (1Sv = 10^6 m^3 s^{-1}). Clockwise circulations are shaded.

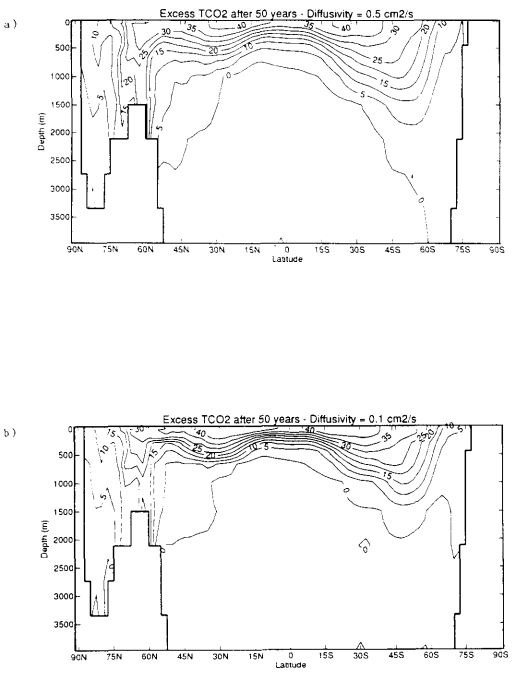

Fig. 18. Meridional sections of zonally-averaged excess T_{CO_2} in μmol kg^{-1} after 50 years of atmospheric emissions for background vertical diffusivities of (a) 0.5 cm^2 s^{-1}, and (b) 0.1 cm^2 s^{-1}. Contour interval is 5 μmol kg^{-1}.

the northern hemisphere where the 10 μmol kg^{-1} isoline has deepened by 300 m at 50°N, and the deeper penetration is particularly noticeable in the Southern Ocean. This rather simple change to the diffusivity coefficient has a dramatic effect on the global uptake of CO_2 by the ocean (Fig. 19). For the first 5 years of emissions the two models take up CO_2 at roughly similar rates. Thereafter, the uptake rates diverge rapidly until by the end of 50 years, the low-diffusivity model is absorbing CO_2 at a rate of 0.4 GtC yr^{-1} less than in the high diffusivity case. A fairly minor reduction in a poorly-known parameter has resulted in a 20% reduction in CO_2 absorption. The stronger flux in experiment B is due partly to enhanced diffusion of CO_2 away from the surface through the thermocline, and partly to the stronger overturning circulation. Fig. 20 shows the difference between the fluxes in experiments B and C for each region. At the time when the emissions into the atmosphere started, enhanced evasion of CO_2

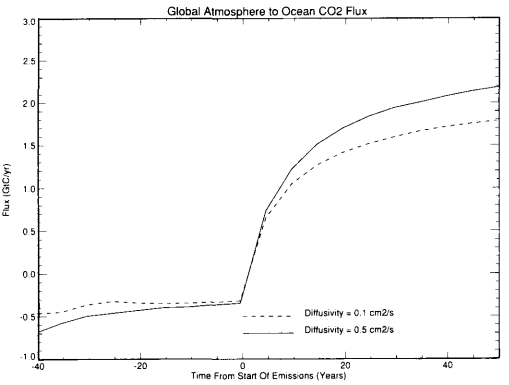

Fig. 19. Comparison between global atmosphere to ocean CO_2 flux for background vertical diffusivities of 0.5 $cm^2\ s^{-1}$ and 0.1 $cm^2\ s^{-1}$.

from the tropics into the atmosphere in experiment B was balanced by stronger invasion south of 15°S. As the runs proceeded, the equatorial and the southern hemisphere regions took up more carbon in experiment B than experiment C, whilst the northern regions showed relatively minor differences. By the end of 50 years the equatorial region accounted for 0.125 GtC yr^{-1}, the Southern Gyres 0.14 and the Antarctic 0.08 GtC yr^{-1} of the total difference between the runs of 0.4 GtC yr^{-1}. This suggests that the major cause of the enhanced uptake is the stronger southern hemisphere meridional circulation induced by higher diffusion.

Which of the two uptake rates is closest to reality? Both runs use diffusivities which are well within the range of those usually employed in

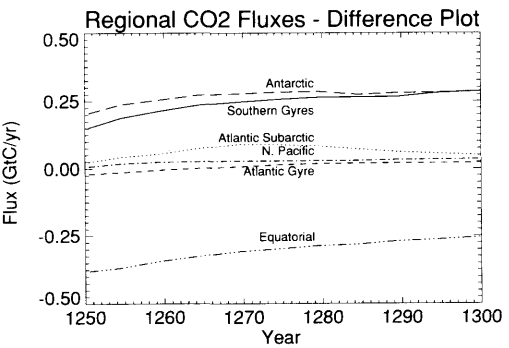

Fig. 20. Time-series of the difference in atmosphere to ocean CO_2 flux for each of the regions defined in Table 3 between experiments B ($\chi_b = 0.5\ cm^2\ s^{-1}$) and C ($\chi_b = 0.1\ cm^2\ s^{-1}$).

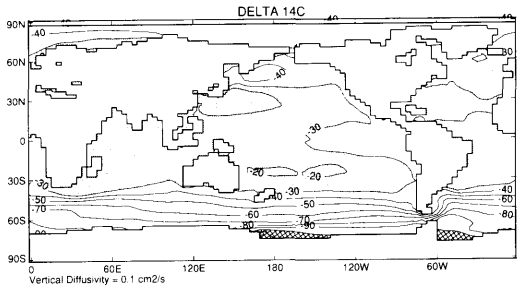

Fig. 21. Predicted $\Delta^{14}C$ ($^o/_{oo}$) at the surface from the low diffusivity run of the model. Contour interval is $10^o/_{oo}$. Values higher than $-30^o/_{oo}$ are lightly stippled. Values lower than $-100^o/_{oo}$ are cross-hatched.

models, but radiocarbon simulations may enable us to place constraints on the estimates. Fig. 21 shows the natural radiocarbon distribution at the surface for the low diffusion experiment, C. Meridional sections from the same run are shown in Fig. 22. These should be compared with the corresponding plots for experiment B, given in Figs. 4 and 5. Surface ^{14}C concentrations are

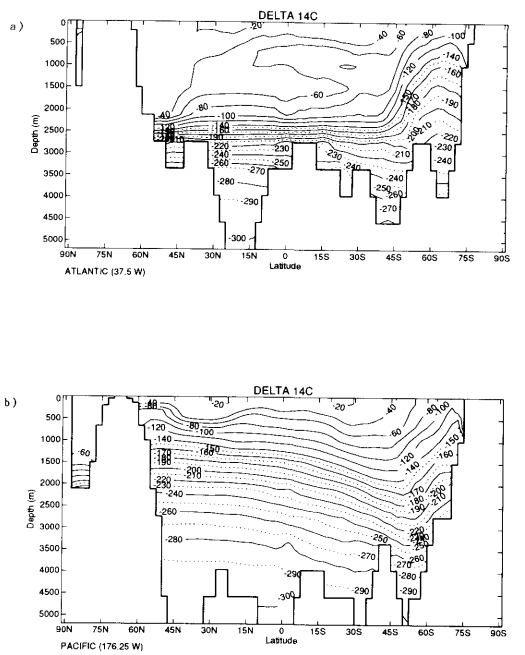

Fig. 22. Predicted latitude-depth cross-sections of $\Delta^{14}C$ ($^o/_{oo}$) through (a) the Atlantic at 37.5°W, and (b) the Pacific at 176.25°W from the low diffusivity run. Solid contours are at intervals of $20^o/_{oo}$. Dotted contours are at intervals of $10^o/_{oo}$ below $-150^o/_{oo}$.

10–20‰ lower in experiment C than experiment B, and the average value for the latitude range 30°S–30°N is −24‰, compared with observations of −40‰. For the low diffusion case, the deep water concentrations are far too low and the observed north–south gradient in the deep Pacific is conspicuously lacking. This is also apparent from a section of zonally-averaged temperature (Fig. 2b). Thus it would appear that experiment C could be discounted on the basis that it is unable to provide a satisfactorily simulation of deep water $\Delta^{14}C$, and that its deep water ventilation characteristics are too sluggish. However, in some ways the low diffusivity simulation is preferable to the high one. The thermocline is shallower and less diffuse, and the radiocarbon distributions above about 2000 m would appear to be more realistic. If it is believed that the region above the thermocline is more important for CO_2 uptake on the timescale of decades, then it could perhaps be argued that the low diffusivity run should provide the better estimate. The use of radiocarbon data to constrain the model is not without ambiguities.

5. Summary and conclusions

In this paper, we have described the development of a three-dimensional model of the ocean's inorganic carbon cycle within the context of an ocean general circulation model. The model is suitable for coupling to an atmospheric general circulation model for studies of climate change and has been designed with this pupose in mind. We presented results from a seasonal simulation of the present-day ocean carbon cycle. The circulation characteristics of the model appear reasonable, but a number of deficiencies in the model have been identified. In common with other GCMs, under conditions of annual mean forcing the model gives North Atlantic Deep Water formation rates that are too low in comparison with deep water of southern origin. It is likely that the use of a more realistic fresh water forcing over the Southern Ocean will improve matters since the forcing dataset employed for these integrations is known to be biased towards summertime values when surface salinities are fresher. The bias towards deep water formation in the southern hemisphere may result in an overestimate of the uptake of CO_2 by the southern oceans. A particular restriction of the model is the neglect of the role of ocean biology in the carbon cycle. Biological processes transfer carbon quite rapidly from surface waters into the deep ocean and are responsible for maintaining much higher concentrations of CO_2 in the deep ocean than is found at the sea surface. The omission of biology has two effects in the model. Firstly, the sharp fall in pCO_2 associated with the spring phytoplankton bloom that is observed in late spring/early summer in the North Atlantic and adjacent seas is not simulated, and summertime partial pressures are consequently too high. Secondly, the model gives deep T_{CO_2} values that are far too low and this means that the high concentrations of CO_2 that are seen at the surface during winter under conditions of deep mixing are similarly not captured by the model. A detailed comparison between the model's simulated surface partial pressures and seasonal observations in high latitudes published by Takahashi et al. (1993) is in consequence rather poor. The model gives lowest partial pressures during winter and highest in summer, since the partial pressure in the model is dominated by the seasonal cycle of sea surface temperature. Meanwhile, observations in high latitude oceans show the opposite, highest values in winter and lowest during summer. Work is in hand to include biology in the next version of the carbon cycle model, and it is anticipated that this will markedly improve the simulation of the present-day carbon cycle.

We investigated the response of the model to a steady increase in anthropogenic CO_2 emissions into the atmosphere over a timescale of 50 years, under conditions of both seasonal and annual-mean forcing. Under seasonal forcing, after 50 years of the perturbation experiment, the ocean is absorbing 2.4 GtC yr^{-1} of the atmospheric emissions of 5.4 GtC yr^{-1}, giving an airborne fraction of 0.56. These figures are similar to those obtained with other ocean models. The comparison of a control and a perturbation experiment allows us to see directly where the excess CO_2 has gone in the ocean. The southern hemisphere is the dominant region for uptake of excess CO_2 - the area south of 15°S accounts for 54% of the total uptake, whilst the northern oceans account for just 25%. This is partly because of the larger area of ocean south of the equator, and partly due to the stronger seasonality of air-sea fluxes in the northern hemisphere compared with the southern

hemisphere - the northern oceans absorb very little anthropogenic CO_2 during late summer. It remains to be seen how these estimates will be changed when biology is included in the model. The Antarctic ocean, south of 50°S, and the equatorial region, between 15°N and 15°S, show the longest response times to the perturbation. Penetration of excess CO_2 below the surface shows quite reasonable agreement with observationally-based estimates. An attempt was also made to compare the model's predicted CO_2 uptake with the estimates of Tans et al. (1990). The agreement was not good, but the comparison was hampered by the non-standard emissions scenario. The method used assumed that the relationship between the CO_2 uptake of different regions is fixed in time, and this assumption is clearly violated (Fig. 14). Also, inclusion of biology would tend to bring the seasonal variation in fluxes in high latitude regions closer to observations. We intend to carry out further experiments using the time-history of atmospheric pCO_2 to force the uptake, both with and without biology. This will enable a more meaningful comparison to be made.

The use of annual mean as opposed to seasonal forcing has surprisingly little effect on global uptake of CO_2. After 50 years of emissions, the two experiments differed by less than 0.1 GtC yr^{-1} in their CO_2 uptake rates. This low sensitivity to the seasonal cycle may be due to the fact that 75% of the excess CO_2 uptake occurs south of 15°N, where the fluxes exhibit little seasonal variation. Again, the inclusion of biology may change this conclusion.

We have also looked at the sensitivity of the model results to variations in the vertical diffusion coefficient, although the high cost of performing lengthy integrations with a GCM has restricted the number of runs that could be done. Lowering the background vertical diffusion coefficient was found to have a much greater effect on the estimated CO_2 uptake. Changing the diffusion coefficient for tracers, within a physically reasonable range, from 0.5 $cm^2 s^{-1}$ to 0.1 $cm^2 s^{-1}$ resulted in a 20% reduction in CO_2 uptake, which was associated with a weaker meridional circulation in the southern hemisphere. The simulation of deep water $\Delta^{14}C$ was very poor in the experiment which used the lowest diffusivity, which suggests that CO_2 uptake estimates based on this run would be too low. However, the simulation above 1000 m was actually improved by reducing the diffusivity. In future, we may be able to improve the model by employing a diffusivity which varies from low values at the surface to higher values in deep water, as in Bryan and Lewis (1979). Simulation of bomb, as opposed to natural, radiocarbon would have been useful in deciding which diffusivity formulation to use, but this was not possible because of the way in which the carbon cyle model was forced. This sensitivity of CO_2 uptake to the choice of a poorly constrained parameter highlights the need for better parameterizations for sub-grid-scale phenomena.

The use of fully three-dimensional models for studies of the carbon cycle is still in its infancy and many improvements and refinements to the models, in terms of both ocean physics and dynamics as well as the carbon cycle models themselves, can be expected in the future. This will eventually lead to improved understanding of the role of the carbon cycle in climate change.

6. Acknowledgements

The author would like to thank three reviewers whose suggestions helped improve the paper significantly. The work described in this article was carried out at the Hadley Centre for Climate Prediction and Research under the UK Department of the Environment Climate Prediction Programme (contract PECD 7/12/37).

REFERENCES

Bacastow, R. B. 1981. Numerical evaluation of the evasion factor. In: *Carbon cycle modelling* (ed. B. Bolin). New York. John Wiley, pp. 95–101.

Bacastow, R. B. and Maier-Reimer, E. 1990. Ocean-circulation model of the carbon cycle. *Clim. Dyn.* **4**, 95–125.

Bottomley, M., Folland, C. K., Hsiung, J., Newell, R. E. and Parker, D. E. 1990. *Global ocean surface temperature atlas (GOSTA)*. A joint project of the Meteorological Office and Dept. of Earth, Atmospheric and Planetary Sciences, Massachusetts Institute of Technology. HMSO, London, 333 pp.

Broecker, W. S. and Peng, T. H. 1982. *Tracers in the sea.* Lamont-Doherty Geological Observatory, Palisades, NY, 690 pp.

Bryan, F. 1987. Parameter sensitivity of primitive equation ocean general circulation models. *J. Phys. Oceanogr.* **17**, 970-985.

Bryan, K. 1969. A numerical method for the study of the circulation of the world ocean. *J. Comput. Phys.* **4**, 347–379.

Bryan, K. 1984. Accelerating the convergence to equilibrium of ocean climate models. *J. Phys. Oceanogr.* **14**, 666–673.

Bryan, K. and Lewis, L. J. 1979. A water mass model of the world ocean. *J. Geophys. Res.* **84**, 2503–2517.

Carrissimo, B. C., Oort, A. H. and Vonder Haar, T. H. 1985. Estimates of the meridional energy transports in the atmosphere and ocean. *J. Phys. Oceanogr.* **15**, 82–91.

Chen, C.-T. A. 1982a. On the distribution of anthropogenic CO_2 in the Atlantic and Southern oceans. *Deep-Sea Res.* **5**, 563–580.

Chen, C.-T. A. 1982b. Oceanic penetration of excess CO_2 in a cross section between Alaska and Hawaii. *Geophys. Res. Lett.* **9**, 117–119.

Cox, M. D. 1984. *A primitive equation, 3-dimensional model of the ocean.* GFDL Ocean Group Tech. Rep. No. 1, 143 pp.

Cox, M. D. 1987. Isopycnal diffusion in a z-coordinate ocean model. *Ocean Modelling* **74**, 1–5.

England, M. H. 1992. On the formation of antarctic intermediate and bottom water in ocean general circulation models. *J. Phys. Oceanogr.* **22**, 918–926.

England, M. H. 1993. Representing the global-scale water masses in ocean general circulation models. *J. Phys. Oceanogr.* **23**, 1523–1552.

Esbensen, S. K. and Kushnir, Y. 1981. *The heat budget of the global ocean: an atlas based on estimates from surface marine observations.* Climate Research Institute, Rep. No. 29, Oregon State University, Corvallis, USA.

Etcheto, J. and Merlivat, L. 1988. Satellite determination of the carbon dioxide exchange coefficient at the ocean-atmosphere interface: A first step. *J. Geophys. Res.* **93**, 15669–15678.

Gargett, A. E. and Holloway, G. 1992. Sensitivity of the GFDL ocean model to different diffusivities for heat and salt. *J. Phys. Oceanogr.* **22**, 1158–1177.

Godfrey, J. S. 1989. A Sverdrup model of the depth-integrated flow for the world ocean allowing for island circulations. *Geophys. Astrophys. Fluid Dyn.* **45**, 89–112.

Goyet, C. and Poisson, A. 1989. New determination of carbonic acid dissociation constants in seawater as a function of temperature and salinity. *Deep Sea Res.* **36**, 1635–1654.

Haney, R. L. 1971. Surface thermal boundary condition for ocean circulation models. *J. Phys. Oceanogr.* **1**, 241–248.

Hellerman, S. and Rosenstein, M. 1983. Normal monthly wind stress over the world ocean with error estimates. *J. Phys. Oceanogr.* **13**, 1093–1104.

Hibler, W. D. 1979. A dynamic-thermodynamic sea-ice model. *J. Phys. Oceanogr.* **9**, 815–846.

Hirst, A. C. and Godfrey, J. S. 1993. The role of Indonesian throughflow in a global ocean GCM. *J. Phys. Oceanogr.* **23**, 1057–1086.

Hsuing, J. 1985. Estimates of global oceanic meridional heat transport. *J. Phys. Oceanogr.* **15**, 1405–1413.

Ineson, S. and Gordon, C. 1989. *Parametrization of the upper ocean mixed layer in a tropical ocean GCM.* Dynamical Climatology Technical Note No. 74. UK Meteorological Office, Bracknell.

IPCC. 1990. *Climate change: the IPCC scientific assessment.* (eds. J. T. Houghton, G. J. Jenkins, and J. J. Ephraums). Cambridge, UK. Cambridge University Press, 365 pp.

Jaeger, L. 1976. Monatskarten des Niederschlags fur die Ganze Erde. *Bet Deutsch Wetterdienstes* **18**, no. 139.

Kraus, E. B. and Turner, J. S. 1967. A one-dimensional model of the seasonal thermocline. II. The general theory and its consequences. *Tellus* **19**, 98–105.

Keeling, C. D., Piper, S. C. and Heimann, M. 1989. A three dimensional model of atmospheric CO_2 transport based on observed winds, 4, Mean annual gradients and interannual variations. In: *Aspects of climate variability in the Pacific and the Western Americas* (ed. D. H. Peterson). Washington, DC. AGU, pp. 305–363.

Keeling, R. F. and Shertz, S. R. 1992. Seasonal and atmospheric variations in atmospheric oxygen and implications for the global carbon cycle. *Nature* **358**, 723–727.

Knaus, J. 1969. A note on the transport of the Gulf Stream. *Deep Sea Res.* **16**, suppl., 117–124.

Levitus, S. 1982. *Climatological atlas of the world ocean.* NOAA Professional Paper 13, US Dept. of Commerce, 173 pp.

Liss, P. and Merlivat, L. 1986. Air-sea gas exchange rates, introduction and synthesis. In: *The role of air-sea exchange in geochemical cycling* (ed. P. Buat-Menard). Dordrecht. D. Reidel, pp. 113–128.

Maier-Reimer, E. and Hasselmann, K. 1987. Transport and storage of CO_2 in the ocean, an inorganic ocean-circulation carbon cycle model. *Clim. Dyn.* **2**, 63–90.

Manabe, S. and Stouffer, R. 1988. Two stable equilibria of a coupled ocean-atmosphere model. *J. Climate* **1**, 841–866.

Marland, G. 1989. *Fossil fuels CO_2 emissions.* CDIAC Communications, Winter 1989, pp. 1–3. Carbon Dioxide Information Analysis Center, Oak Ridge National Laboratory, Oak Ridge, Tenn.

Mehrbach, C., Culberson, C. H., Hawley, J. E. and Pytkowicz, R. M. 1973. Measurement of apparent dissociation constants of carbonic acid in seawater at atmospheric pressure. *Limnol. Oceanogr.* **18**, 897–907.

Murphy, J. 1994. Transient response of the Hadley Centre coupled ocean-atmosphere model to increasing

carbon dioxide. Part I. Control climate and flux correction. *Journal of Climate*, in press.

Nowlin, W. D. Jr. and Klinck, J. M. 1986. The physics of the Antarctic Circumpolar Current. *Rev. Geophys.* **24**, 469–491.

Pacanowski, R. C. and Philander, S. G. H. 1981. Parameterization of vertical mixing in numerical models of tropical oceans. *J. Phys. Oceanogr.* **11**, 1443–1451.

Pearman, G. I., Hyson, P. and Fraser, P. J. 1983. The global distribution of atmospheric carbon dioxide. *J. Geophys. Res.* **88**, 3581–3590.

Peng, T.-H., Takahashi, T. and Broecker, W. 1987. Seasonal variability of carbon dioxide, nutrients and oxygen in the northern North Atlantic surface water: observations and a model. *Tellus* **39B**, 439–458.

Redi, M. H. 1982. Oceanic isopycnal mixing by coordinate rotation. *J. Phys. Oceanogr.* **12**, 1154–1158.

Roberts, D. L. and Cattle, H. 1989. *Simulation of sea-ice in a coupled ocean-atmosphere model.* Dynamical Climatology Technical Note no. 85. UK Meteorological Office, Bracknell.

Sarmiento, J. L., Orr, J. C. and Siegenthaler, U. 1992. A perturbation simulation of CO_2 uptake in an ocean general circulation model. *J. Geophys. Res.* **97**, 3621–3645.

Semtner, A. J. 1976. A model for the thermodynamic growth of sea ice in numerical investigations of climate. *J. Phys. Oceanogr.* **6**, 379–389.

Takahashi, T., Olafsson, J., Goddard, J. G., Chipman, D. W. and Sutherland, S. C. 1993. Seasonal variation of CO_2 and nutrients in the high latitude oceans: a comparative study. *Global Biogeochemical Cycles* **7**, 843–878.

Tans, P. P., Fung, I. Y. and Takahashi, T. 1990. Observational constraints on the global atmospheric CO_2 budget. *Science* **247**, 1431–1438.

Taylor, N. K. 1992. The role of the ocean in the global carbon cycle. Part 2: Climate feedbacks. *Weather* **47**, 237–241.

Thomas, F., Perigaud, C., Merlivat, L. and Minster, J. F. 1988. World scale monthly mapping of the CO_2 ocean-atmosphere gas transfer coefficient. *Philos. Trans. R. Soc. London Ser.* **A325**, 71–83.

Toggweiler, J. R., Dixon, K. and Bryan, K. 1989. Simulations of radiocarbon in a coarse-resolution, world ocean model. I. Steady state, pre-bomb distributions. *J. Geophys. Res.* **94**, 8217–8242.

Wanninkhof, R. 1992. Relationship between wind speed and gas exchange over the ocean. *J. Geophys. Res.* **97**, 7373–7382.

Yin, F. L. and Fung, I. Y. 1991. Net diffusivity in ocean general circulation models with nonuniform grids. *J. Geophys. Res.* **96**, 10773–10776.